RESEARCH ARTICLE

A Hydride Migration Mechanism for the Mo-Catalyzed *Z*-2-Selective Isomerization of Terminal Alkenes

Sarah E. Jenny,[a] Juan M. Serviano,[a] Ainara Nova,*[b] and Graham E. Dobereiner*[a]

[a] Dr. Sarah E. Jenny, Juan M. Serviano, Prof. Dr. Graham E. Dobereiner
Department of Chemistry
Temple University
Beury Hall, 1901 N 13th St, Philadelphia, PA, 19122
E-mail: dob@temple.edu; Homepage: https://www.doblab.org

[b] Prof. Dr. Ainara Nova Flores
Department of Chemistry, Hylleraas Centre for Quantum Molecular Sciences and Centre for Materials Science and Nanotechnology
University of Oslo
Blindern, P.O. Box 1033, 0315 Oslo, Norway
E-mail: a.n.flores@kjemi.uio.no

Supporting information for this article is given via a link at the end of the document.

Abstract: The catalytic one-bond isomerization (transposition) of 1-alkenes is an emerging approach to *Z*-2-alkenes. Design of more selective catalysts would benefit from a mechanistic understanding of factors controlling *Z* selectivity. We propose here a reaction pathway for *cis*-$Mo(CO)_4(PCy_3)$(piperidine) (**3**), a precatalyst that shows high *Z* selectivity for transposition of alpha olefins (e.g., 1-octene to 2-octene, 18:1 *Z*:*E* at 74% conversion). Computational modeling of reaction pathways and isotopic labeling suggests the isomerization takes place via an allyl (1,3-hydride shift) pathway, where oxidative addition of *fac*-$(CO)_3Mo(PCy_3)(\eta^2$-alkene) is followed by hydride migration from one position (*cis* to allyl C^3 carbon) to another (*cis* to allyl C^1 carbon) via hydride/CO exchanges. Calculated barriers for the hydride migration pathway are lower than explored alternative mechanisms (e.g., change of allyl hapticity, allyl rotation). To our knowledge, this is the first study to propose such a hydride migration in alkene isomerization.

Introduction

Selective alkene isomerization reactions[1–18] and related tandem isomerization/functionalization reactions[19,20] can rapidly generate molecular complexity. Through catalyst control, specific regio- and stereoisomers can be achieved in several reaction contexts.[21] Reactions for selectively accessing *Z* (cis) alkenes are hindered by the greater thermodynamic stability of *E* (trans) isomers. A few *Z*-selective approaches overcome the thermodynamic preference for *E* and offer facile access to *Z* alkenes of synthetic value, including thermal[15,22–28] and photocatalytic *E*-to-*Z* methods.[29–31] The one-bond transposition, or isomerization, of 1-alkenes to *Z*-2-alkenes[2,4,9,32–36] is a promising approach (Scheme 1).[37] However, while one-bond alkene transposition of 1-alkenes is energetically downhill, targeting specific isomers remains a challenge. Overisomerization[25] is common and selectivity is substrate dependent.

Understanding the factors controlling selectivity will aid the rational design of improved isomerization catalysts. Selectivity in isomerization explored in mechanistic studies[2,3,8,33,34,38] has led to proposals[39–41] invoking alkyl (via 1,2-insertion & β-H elimination) and allyl (via 1,3-hydride shift) pathways (Figure 1).[42]

Z-2-alkenes through isomerization (one-bond transposition)

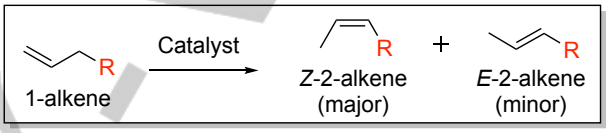

Scheme **1.** *Z*-2-selective isomerization of 1-octene.

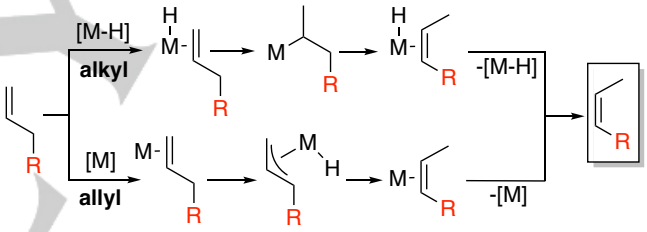

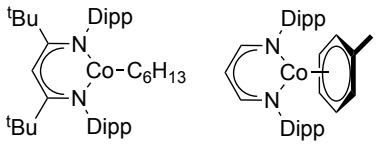

A *alkyl mechanism* **B** *allyl mechanism*

Figure 1. Top: Alkyl and allyl mechanisms for one-bond transposition. For clarity, only the *Z* isomer product is shown. Bottom: Structures of Z-selective Co(II) catalyst **A** and Co(I) catalyst **B**, which were proposed to operate through different isomerization mechanisms by Holland and coworkers.

For example, based on isotopic labelling studies and observation of 3- and 4-alkene products resulting from alkene chain walking, *Z*-selective Co(II) catalyst **A** (Figure 1)[33] was proposed by Holland and coworkers to proceed through an alkyl route via selectivity-determining β-H elimination. In contrast, Holland and coworkers[2] used DFT to propose Co(I) catalyst **B** operates via an allyl mechanism, with oxidative addition serving as the selectivity-determining step.

Parallel work in our lab has identified alternative catalytic methods. Mo(0) precatalyst *cis*-$Mo(CO)_4(PPh_3)_2$ (**C**) achieves moderate *Z* selectivity in the presence of an acid co-catalyst.[4]

Since **C** uses simple ligands and can be prepared on gram scale – of value in industrial applications – we have sought similar precatalysts that achieve higher Z selectivity. Although facile ligand exchange during catalysis with **C** frustrated our attempts to observe intermediates *in situ* in support of a mechanistic proposal, we hypothesized that 7-coordinate Mo(II) hydride species were plausible intermediates on an allyl-type reaction pathway.

Unlike 6-coordinate (octahedral) compounds, a 7-coordinate intermediate must rearrange for subsequent C–H bond formation and release of product. In one such sequence (Scheme 2A) product forms via reductive elimination to a Mo(0) complex. In evaluating stereoisomerization (rearrangement) mechanisms we considered that CO ligands may enable rearrangement by assisting hydride migration, either via formyl intermediates[43,44] or via pseudorotation. In an example of the latter, Kirchner and co-workers[45] calculate that 7-coordinate $[M(PNP)(CO_3)H]^+$ (M = Mo, W) achieves a single-step interconversion (pseudorotation) of adjacent CO and hydride ligands (Scheme 2B). For a Mo(II) hydride in an allyl-type isomerization, multiple rearrangements would achieve the stereochemistry needed for reductive elimination, achieving 2-alkene product (Scheme 2A).

Here, we present a mechanistic proposal for the *Z*-selective isomerization of a well-defined catalyst precursor – *cis*-$Mo(CO)_4(PCy_3)$(piperidine) (**3**) – that features rearrangement of Mo–H via assistance of CO ligands, without involvement of a formyl intermediate. Based on DFT analysis, we propose positional isomerization to form *Z* product is achieved via two consecutive rearrangements, with *Z*-selectivity the result of differences in steric pressure throughout the pathways that lead to the *E*-2 and *Z*-2 alkene products.

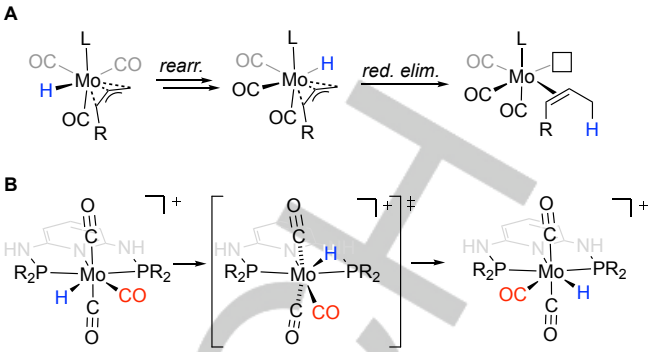

Scheme 2. A: Rearrangement and reductive elimination from a 7-coordinate Mo intermediate, forming a *Z*-2-alkene product bound to octahedral Mo(0). **B:** Pseudorotation proposed by Kirchner and co-workers.

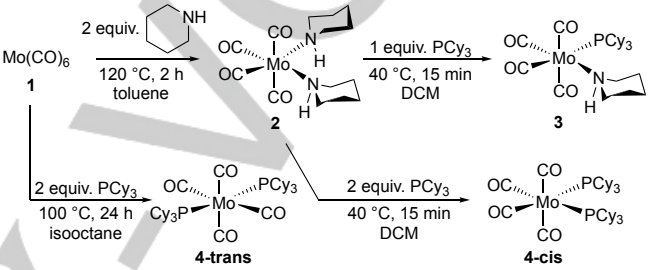

Scheme 3. Synthesis of select Mo(0) species for isomerization.

Results and Discussion

Evaluation of Isomerization Precatalysts

We attempted one-bond transposition of 1-octene using *cis*-$Mo(CO)_4(PCy_3)_2$ (**4-*cis***, Scheme 3)[46] as a precatalyst, thinking the bulky, electron rich PCy_3 may yield a catalyst more selective than previously-studied $Mo(CO)_4(PPh_3)_2$. As in our prior report,[4] **4-cis** was screened in the presence of an acid (diphenyl phosphate; dpp). Conversion and selectivity with **4-*cis*** as initially prepared were batch dependent. Once recrystallized, **4-*cis*** was poorly active (Table 1). Further analysis of ^{31}P NMR spectra of early **4-*cis*** batches led to identification of impurity *cis*-$Mo(CO)_4(PCy_3)$(piperidine) (**3**),[47] presumably an intermediate in the synthesis of **4-*cis*** (Scheme 3). Isolated and purified **3** is far more active than **4-*cis***, **4-trans**, or $Mo(CO)_5(PCy_3)$ (**5**) (Table 1). While *cis*-$Mo(CO)_4$(piperidine)$_2$ (**2**) shows poor selectivity (Table 1, entry 2), adding 1 equiv. PCy_3 to the reaction resulted in 92% conversion, 10.7:1 *Z*:*E* with 10% higher (3- and 4-) alkenes using 1-octene. Since **3** is simple to make and purify with excellent reproducibility, we explored the catalytic mechanism using **3** as precatalyst.

Table 1. Isomerization of 1-octene with various Mo complexes using diphenyl phosphate as acid additive.[a]

Entry	Complex	dpp (mol %)	Conversion	Selectivity (*Z*:*E*)
1	**1**	15	0%	n/a
2	**2**	1.5	50%	2.4 : 1
3	**3**	0	18% (1%)	3.4 : 1
4	**3**	1.5	74%	18.0 : 1
5	**3**	15	34%	7.1 : 1
6	**4-trans**	15	12%	1.7 : 1
7	**4-cis**	15	9% (1%)	13.0 : 1
8	**5**	15	trace	n/a

[a] Isomerization of 1-octene using 1.5 mol% complex and diphenyl phosphate (dpp). Combined conversion to 3- and 4-alkenes shown in parentheses. Data is the average of three trials after 1 h at 80 °C in C_6D_6. Analysis done via ^1H NMR.

Formation of the Active Species

In our prior system[4] (Mo(0) precatalyst **C**, Figure 1), optimal conversion and selectivity was achieved with a 10:1 ratio of acid to Mo. Here, a 1:1 ratio of acid to Mo (dpp:**3**) results in high activity (Table 1, entry 4); contrast with **4**, where even 10:1 dpp:**4** is insufficient to achieve comparable activity (entries 6-7). We hypothesized that piperidine (pip) is more easily protonated than PCy_3 in creating the vacant site needed for catalyst activity. To explore further, DFT models of **2**, **3**, and **4-*cis*** were geometry optimized (structures **I2**, **I3**, and **I4**, respectively) and thermochemistry of their reaction with dpp calculated (M06-GD3/def2TZVP//M06-GD3/def2SVP with SMD solvation; Scheme 4).

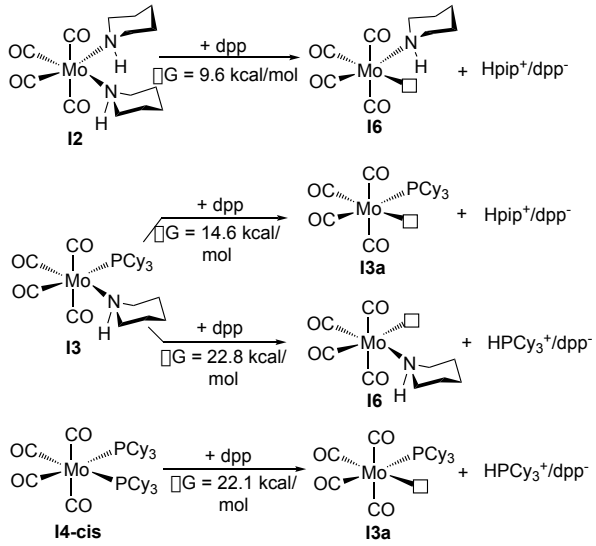

Scheme 4. Free energies (in kcal/mol) of initiation pathways. dpp = diphenyl phosphate; pip = piperidine.

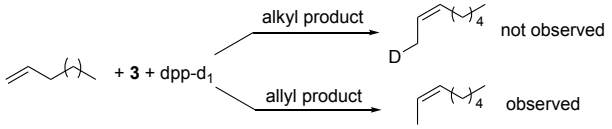

Scheme 5. Expected products for alkyl versus allyl pathways in transposition catalysis of 1-alkenes with **3** and diphenyl phosphate-d_1. In experiment, only the unlabeled product (bottom pathway) was observed, suggesting an allyl mechanism is operating for catalyst **3**.

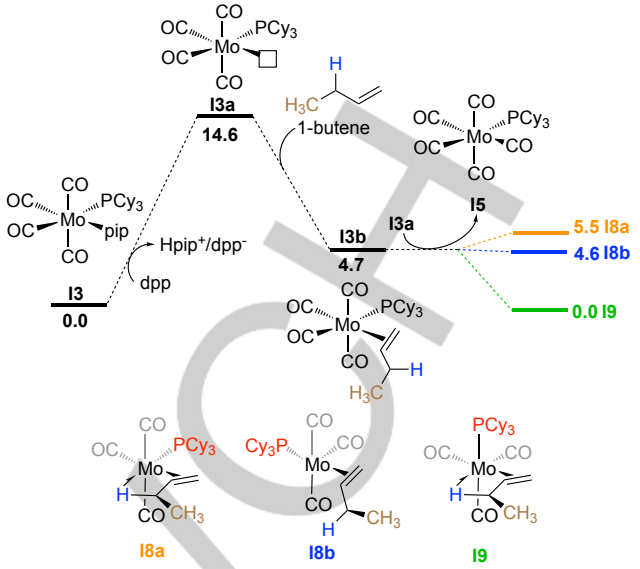

Scheme 6. Free energies (in kcal/mol) of intermediates before and after CO transfer from **I3b** to **I3a** forming **I5** and η^2 olefin complexes **I8a**, **I8b**, and **I9**.

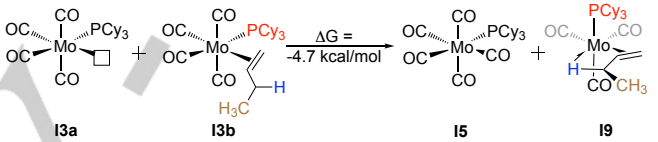

Scheme 7. Initiation of **I3**, forming **I9** with concurrent formation of **I5**.

Salt precipitation is observed experimentally, likely driving the reaction forward; therefore, the absolute free energies are challenging to predict via DFT.[48] However, formation of piperidinium diphenyl phosphate ([Hpip][dpp]) from dpp and **I2** or **I3** requires relatively less free energy (9.6 and 14.6 kcal/mol with **I2** and **I3**) than the protonation of **I3** and **I4-*cis*** to form [$HPCy_3$][dpp] (>22.0 kcal/mol with **I3** and **I4-*cis***). Since Cortés-Figueroa and coworkers[47] observed facile, reversible piperidine dissociation from **3** in chlorobenzene, protonation of piperidine in the present system may occur after it dissociates from Mo. If indeed **4-cis** and **3** lead to a common *Z*-forming active species, the lower catalytic activity and selectivity of **4-*cis*** compared to **3** (Table 1) could be due to slow activation, where, for example, the unwanted secondary isomerization of 2-*Z* product to *E* alkene (vide infra) becomes kinetically competitive. However, more kinetic data would be required to establish a common active catalyst for these precatalysts.

Consideration of an Allyl vs. Alkyl Mechanism

With the protonation of piperidine to create a vacant site, multiple next steps are possible. Since the second-row (Mo) complexes here feature strong-field ligands (CO, PCy_3), we focused on alkyl and allyl-based mechanisms (e.g., Figure 1) over radical[49] pathways. Our primary focus was on assessing alkyl and allyl pathways. Before proceeding with DFT calculations, we attempted catalytic reaction of **3** using isotopically labeled diphenylphosphate-d_1 (dpp-d_1). If an alkyl pathway were operating, formation of a metal deuteride followed by olefin insertion would generate a C–D bond (Scheme 5; see SI for spectra) suggests the acid does not enable an alkyl mechanism via M–H(D) formation. We further reasoned that cationic intermediates in an alkyl mechanism would be disfavored in the benzene medium used in catalysis (verified by DFT calculations; see SI). For these reasons, our computational efforts focused on viable allyl mechanisms with **3**. We note here that all pathways were explored computationally using 1-butene as a substrate, since its lower conformational entropy versus other 1-alkenes greatly simplifies modeling of the mechanism.

In an allyl mechanism, substrate binds to the site left vacant by piperidine, forming an η^2 olefin complex (e.g., **I3b**, Scheme 6). Next, a second ligand dissociates so that C–H bond oxidative addition can take place. Loss of a CO from **I3b** directly results in a *fac* (**I9**) or *mer* (**I8a**) orientation of the remaining CO ligands. Another *mer* species **I8b** would be formed via CO loss followed by rearrangement. While other η^2 olefin complexes are possible, we focus here on the three (**I8a**, **I8b**, and **I9**) that can directly undergo C-H oxidative addition.

Although CO dissociation is endergonic by more than 20 kcal/mol, transfer of CO from one complex to another is exergonic and can drive the reaction. For example, reaction of **I3b** and **I3a**, yielding **I5** and **I9**, is exergonic by 4.7 kcal/mol (Scheme 7). Indeed, CO transfer is observed in catalytic reactions of **3** via ^{31}P NMR, with $Mo(CO)_5(PCy_3)$ (**5**) the most abundant Mo-P containing species. The *fac* isomer (**I9**) has the lowest energy of the three possible species (Scheme 6), but the energy difference between *fac* and *mer* are small enough that all should be accessible *in situ*. For this reason, **I8a**, **I8b**, and **I9** were examined for their relative barriers towards oxidative addition.

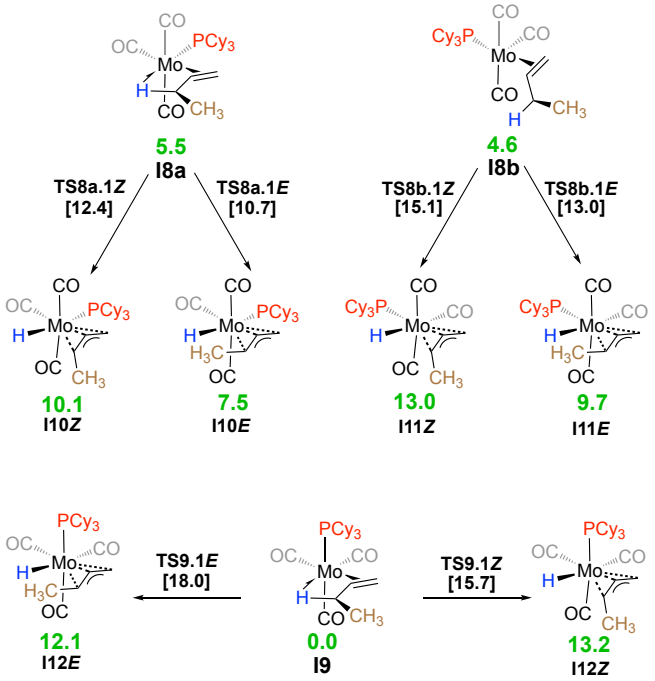

Scheme 8. Free energies (in kcal/mol) of oxidative addition of 1-butene with **I8a**, **I8b**, and **I9.**

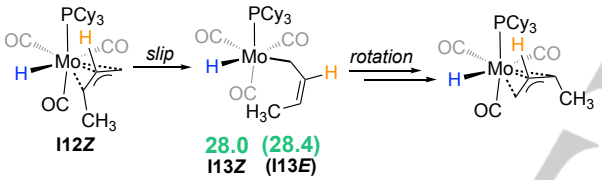

Scheme 9. Scheme showing an allyl slip and rotation pathway to enable reductive elimination at the C^1 carbon. For **I12Z**, the slip forming **I13Z** is endoergic by 28.0 kcal/mol. For **I12*E***, it is 28.4 kcal/mol to reach **I13*E***.

Insight into the Allyl Mechanism: Oxidative Addition

Oxidative addition of the C^3–H bond by **I8a**, **I8b**, or **I9** forms 7-coordinate Mo(II) η^3-allyl hydrides, with allyl geometries that can lead to either a *Z*- or *E*-2-alkene (Scheme 8). In the case of the *mer* species (**I8a** and **I8b**), the transition state energies are higher for the *Z* isomer than the *E*, while for fac species **I9**, the transition state energy is lower for the *Z* isomer (**TS9.1*Z***) than the *E* (**TS9.1*E***) by 2.3 kcal/mol. Given the small energy differences between **I10*Z*/*E***, **I11*Z*/*E***, and **I12*Z*/*E***, we calculated reaction pathways from each (See SI for full details).

Insight into the Allyl Mechanism: Rearrangement

After oxidative addition, a rearrangement is needed to bring the C^1 allyl carbon proximal to hydride for subsequent reductive elimination (Scheme 2A). Allyl rotation would achieve the needed geometry but attempts to find a TS for an allyl rotation from **I10**, **I11**, or **I12** were all unsuccessful. Unlike Cp* ring rotation, which can be quite rapid for Mo(II) hydrides,[50] prior computational studies have found Mo allyl rotation requires stabilization from *trans* ligands,[51] use of allene precursors,[52] and/or very low steric

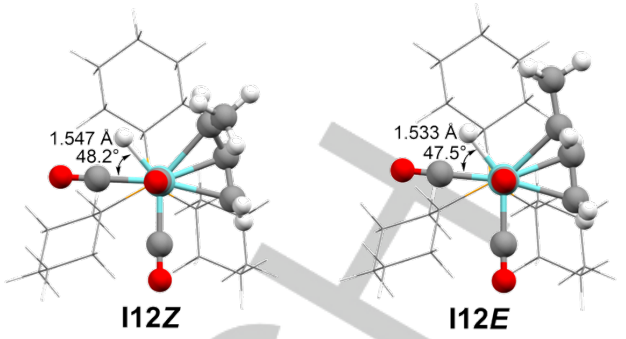

Figure 2. H-to-C distances (in Angstroms) and OC–Mo–H angles in **I12*Z*** (left) and **I12*E*** (right). PCy_3 shown in wireframe for clarity.

hindrance,[53] none of which are available in the current system. Alternatively, η^3/η^1 allyl slippage would allow for rotation of the substrate.[45,54] While a mechanism was found by DFT, energies were unreasonably high for this process (Scheme 9). The η^1 allyl *intermediate* was 4 kcal/mol higher than the lowest *transition states* for *E*/*Z* pathways for H migration mechanisms (*vide infra*).

Unable to find a energetically reasonable allyl rotation or allyl slip pathway, we considered hydride migration[45] of **I10*E*/*Z***, **I11*E*/*Z*** and **I12*E*/*Z*** through the assistance of CO ligands. The inspiration for this approach came from the short H to CO distances and small OC–Mo–H angles observed in **I12*E*** and **I12*Z*** (Figure 2), where the hydrogen-to-carbon distances are <1.55 Å and H–Mo–C angles are approximately 48°. For comparison, Kirschner and coworkers[45] found solid-state [Mo(PNPMe-*i*Pr)$(CO)_3$H]BF_4 – a complex which undergoes pseudorotation (Scheme 2B) – to possess a H to equatorial C_{CO} distance of 1.62 Å and a H–Mo–C angle of 52°. The W congener showed a H–C Wiberg index of 0.20, which Kirchner and coworkers suggested reflects an attractive interaction between H and C_{CO} . From NBO analysis of our complex **I12*Z***, a H–C Wiberg index of 0.35 similarly suggests an attractive interaction between H and C_{CO}. The acceptor CO shows the expected slight lengthening, with a C–O Wiberg index of 1.95, relative to the 2.06 and 2.08 for the other COs. If an attractive H/CO interaction is enabling pseudorotation in the Kirschner system, **I12*E*** and **I12*Z*** may exhibit similar reactivity. Note **I12*Z*** has a shorter hydrogen-to-carbon distance (1.547 Å) and a longer H–Mo bond (1.788 Å) than, for example, **I11*Z*** (2.626 and 1.758 Å, respectively; see Table S1 for details), suggesting the geometry of the isomer formed upon oxidative addition dictates the magnitude of the H/CO interaction.

We searched for hydride migration pathways starting from **I8a**, **I8b,** and **I9** (Calculated intermediates and transition states on all explored pathways can be found in the SI). In all cases, more than one pseudorotation is needed for the hydride to move from the starting position adjacent to the C^3 carbon to the ending position next to the C^1 carbon. For *fac* structure **I9**, the highest barriers on productive pathways are 24.2 kcal/mol (leading to *Z*; Scheme 10) and 25.1 kcal/mol (leading to *E*). On the *Z*-leading pathway, the first of two successive hydride migrations (**TS9.2*Z***; 24.2 kcal/mol) has a slightly higher energy than the second (**TS9.3*Z***; 23.9 kcal/mol). For the *E*-leading pathway, the relative energies are reversed; the first migration (**TS9.2*E***; 20.1 kcal/mol) is lower than the second (**TS9.3*E***; 25.1 kcal/mol).

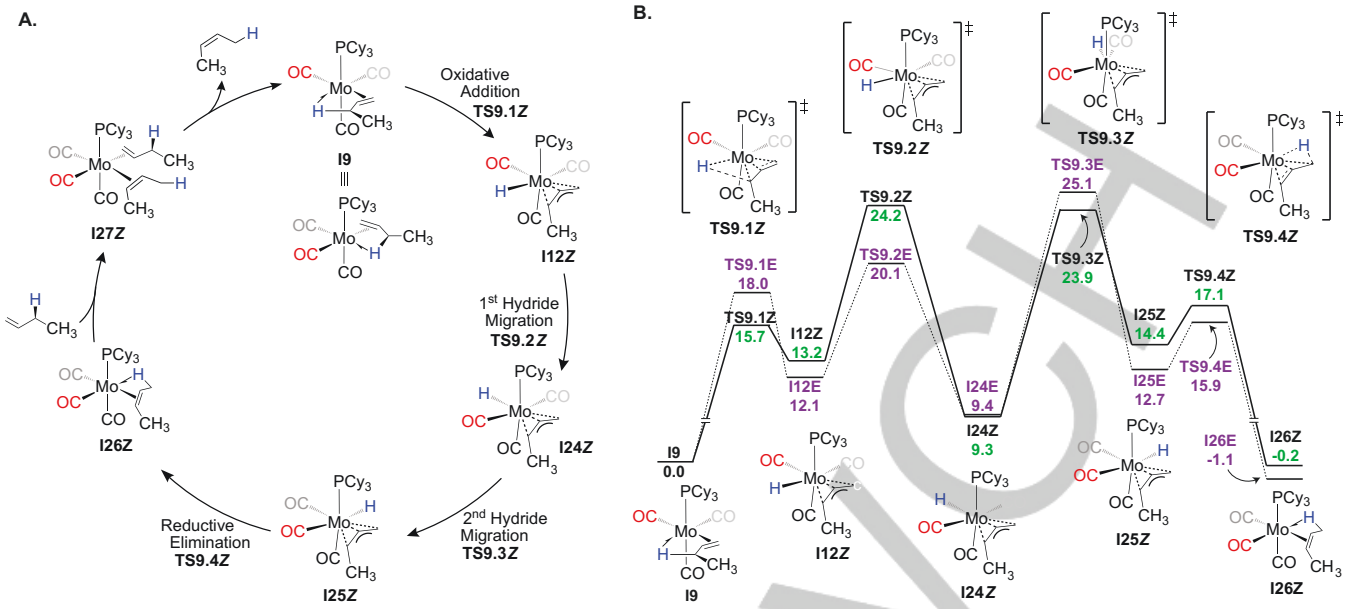

Scheme 10. A. Proposed *Z*-2-alkene catalytic cycle with two hydride migration (pseudorotation) steps occurring between oxidative addition and reductive elimination. **B.** Free energies (in kcal/mol) of intermediates and transition states along pathways from intermediate **I9**. Structures along the Z-leading pathway are pictured, with their energies in green; energies for structures along the E-leading pathway are shown in purple. All structures can be found in the Supporting Information.

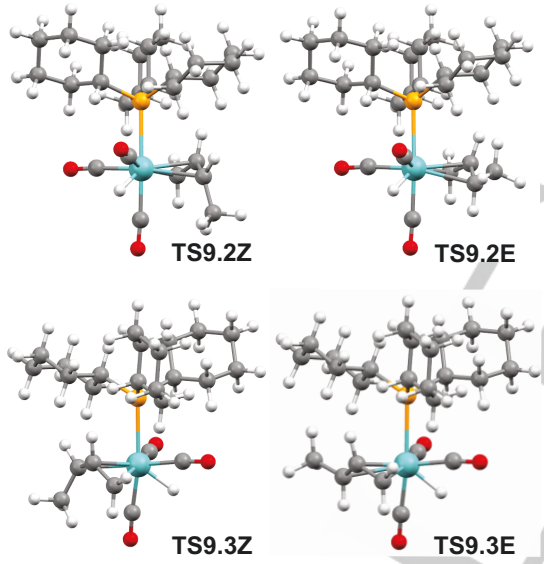

Figure 3. Transition state geometries for hydride migration steps.

Pathways from **I8a** and **I8b** are higher in energy. *fac* CO orientations are electronically preferred when sterics allow it,[55–57] perhaps accounting for the lower energy of the **I9** pathway vs. **I8a** and **I8b**. Also, pathways from *mer* structures **I8a** and **I8b** must complete an additional step: distortion to a semi-*fac* orientation to achieve a geometry for productive reductive elimination. In the case of **I8a**, **TS8a.2Z** is the highest barrier on the *Z*-alkene forming path, at 27.3 kcal/mol relative to **I3**, while for the *E* path, **TS8a.2*E*** is similar, at 26.9 kcal/mol. Compared to **I8a**, barriers are higher for **I8b**, because of steric clash between allyl Me and PCy_3 (28.0 kcal/mol for **TS8b.4Z**, 26.9 for **TS8b.4*E***).

Comparing the highest energy transition states from **I9** offers an explanation for the observed preference for the formation of *Z*-2-alkenes over *E*-2 (Figure 3).[58] Differences in energy are in part due to the steric pressure of the *syn* or *anti* methyl of the allyl ligand. Since the *fac* CO orientation of the lowest-energy (**I9**) pathways position the allyl *cis* to PCy_3, there are close allyl/PCy_3 contacts in the four hydride migration transition states. During the first H migration, the closest is the *meso* hydrogen atom of the allyl and the axial C-H atom of PCy_3: 1.89 Å (**TS9.2*E***) and 1.91 Å (**TS9.2*Z***). In the second hydride migration, the Mo–P bond is elongated (2.70 Å) in **TS9.3*E*** compared to **TS9.2*E*** (2.66 Å), which more resembles **TS9.2*Z*** (2.66 Å), and **TS9.3*Z*** (2.67 Å). The sum of steric influences between ligands appears to play a role in favoring one alkene isomer over another; however, no single variable stands out as the chief determinant of Z selectivity

Once hydride migration has occurred, reductive elimination yields a η^2-alkene complex with an additional agostic interaction between alkene and Mo. The introduction of a second equivalent of substrate promotes the loss of product alkene (Scheme 10). The barriers observed for these steps are significantly lower than those of the hydride migration and were judged unlikely to strongly influence rate or selectivity (see SI).

From DFT, routes via *fac* CO complex **I9** therefore appear to be the most reasonable pathways for formation of *Z*-2-alkenes using precatalyst **3**. Hydride migration facilitated by CO provides a mechanism that is energetically accessible and qualitatively consistent with the selectivity observed in experiments. We interpret the free energy difference between **TS9.2*Z*** and **TS9.3*E*** as the combined effect of several steric interactions. We caution that the 1-butene model, used to reduce the computational cost, cannot be used to quantitatively predict *Z* selectivity for the studied substrates experimentally (vide infra). However, the linear elongation of the alkane chain should not change the preferred isomer due to its location far from the phosphine ligand.

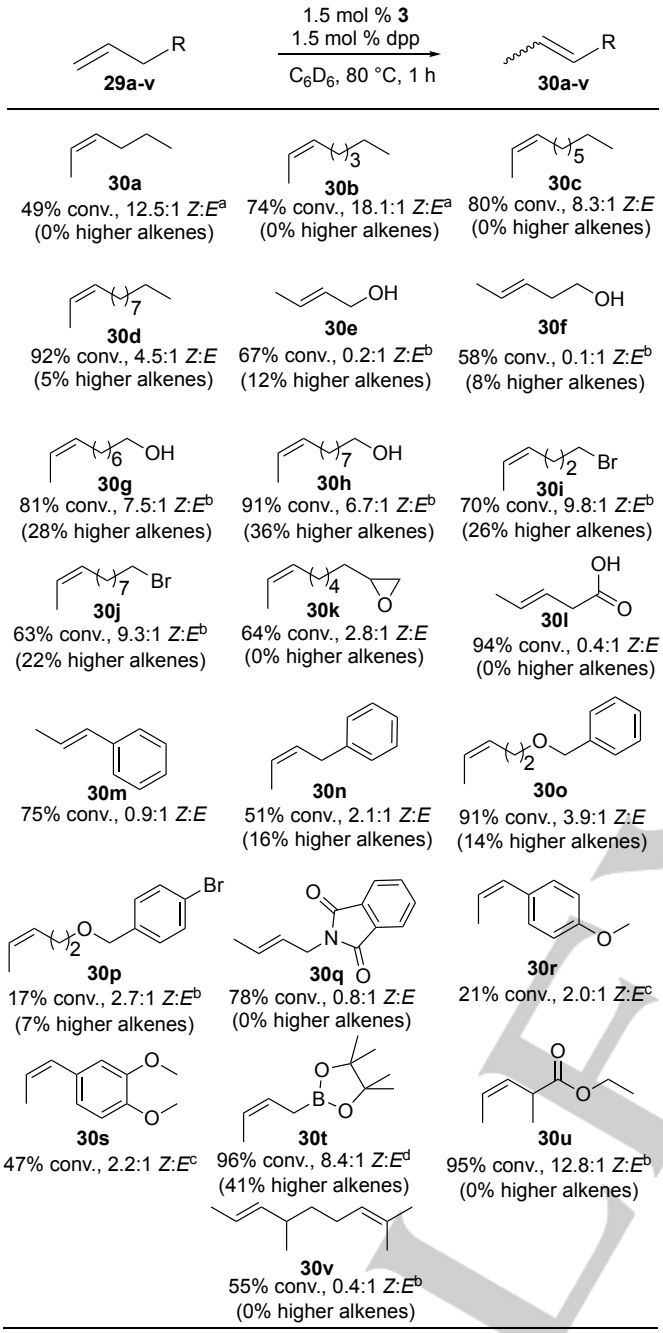

[a] 0.15 mol% [Mo]; 0.15 mol% dpp
[b] *Z*:*E* and higher alkene content determined by ^{13}C NMR - see SI for details
[c] 2 mol% [Mo]; 2 mol% dpp
[d] Value obtained from a single trial

Scheme 11. Substrates isomerized using **3** and dpp.

Substrate Dependence on Isomerization Selectivity

To better understand the role of substrate on selectivity, a scope was explored using **3** as precatalyst. Reactions with **29a-v** were performed at NMR-tube scale and conversions of **30a-v** determined as an average of three trials (Scheme 11).

Conversions between 60-80% are reached for most substrates in 1 h at 80 °C. Because the kinetic *Z*-2-alkene product can undergo a slower, subsequent, *Z*-to-*E* isomerization, *Z* selectivity is sensitive to both catalyst loading and reaction times. For example, 1-hexene, at 0.15 mol% **3** and 0.15 mol% dpp, provides 49% *Z*-2-hexene (**30a**) with 12.5 *Z*:*E*; *increasing* catalyst loading and acid loading to 0.2 mol% increases conversion of 69% but at the expense of selectivity (6.7:1 *Z*:*E*). This trend is also visible with 1-dodecene to form **30d**. *Decreasing* the catalyst loading from 1.5 mol% to 1 mol% reduces conversion of 67% with an increase in selectivity (6.7:1 *Z*:*E*-2-alkene, and only trace quantities of other isomers, e.g., 3-dodecene). Therefore, catalysis with **3** can be used to target either high conversion or high selectivity by varying the relative amount of catalyst and acid to substrate.

Exploring functional group tolerance shows that certain motifs erode selectivity. Short-chain ω-alcohols (**29e**, **29f**) isomerize to thermodynamic ratios. 3-buten-1-ol (**29e**), for example, forms with selectivity of 0.2:1 *Z*:*E* while the thermodynamic *Z*:*E* is 0.152:1.[59,60] However, longer chain alcohols (**29g** & **29h**) show much higher *Z* selectivity. One possible explanation is that shorter-chain alcohols can chelate to the metal center and engage the catalyst in other, less selective, mechanisms. Trace quantities of aldehyde are formed with **29e** – consistent with isomerization/tautomerization – but not observed in **29f**-**29h**.

Other alkyl functional groups tended not to have the same pitfalls as the alcohols. ω-brominated 1-alkenes gave similar conversion and selectivity for the two chain lengths tested (5 carbons, **29i**: 70%, 9.8:1 *Z*:*E*; 11 carbons, **29j**: 63%, 9.3:1 *Z*:*E*). Catalysis with **3** is also compatible with epoxide **29k**, showing good conversion with modest selectivity (2.8:1 *Z*:*E*). Carboxylic acid (**29l**) gave good conversion (94%) and no α, β-unsaturated product but poor selectivity (0.4:1 *Z*:*E*). As with the short-chain alcohols, chelation may be the cause of the low selectivity observed for **29l**.

Substituted arenes yielded lower *Z* selectivity than aliphatic substrates. Allyl benzene (**29m**) had good conversion (though lower than for prior catalysts **A** and **B**) with relatively poor selectivity (close to 1:1 *Z*:*E*) albeit much higher than the thermodynamic ratio (0.03:1 Z:E).[61] Better conversion was observed with homoallylic **29n**, but here the strong thermodynamic preference for the conjugated styrenyl product resulted in 16% of the two-bond isomerization product. For aryl substrates, lowering the catalyst loading did not improve selectivity.

Two benzyl ethers – one halogenated in the *para* position – were also tested to show the effect of a distal electron withdrawing group on isomerization. Without the electron withdrawing group (**29o**), we observe high conversion (91%) with a substantial amount of higher alkene isomers (14%) compared to other substrates. When a *para*-bromo substituent is added (**29p**), conversion drops significantly to 17%. In either case, *Z* selectivity remains modest (2.7:1 *Z*:*E* without bromo, 3.1:1 *Z*:*E* with). Good conversion with low selectivity was observed in the case of **29q**, with low conversion for substrates **29r** and **29s**.

Three substrates containing Bpin (**29t**), ester (**29u**), and diene (**29v**) functionality were of particular interest given their potential synthetic value in subsequent transformations. In the case of **29t** the selectivity of 8.4:1 *Z*:*E* is slightly higher than our 2018 system but over-isomerization has increased (41% versus 9%). Much to our excitement, **29u** isomerized to 95% conversion with good selectivity (12.8:1 *Z*:*E*) and no observable over-isomerization. Finally, an unconjugated diene resulted in moderate conversion (55%) with 0.4:1 *Z*:*E* (**29v**). For both **29u**

and **29v**, the potentially chelating nature of the substrates could be influencing selectivity.

Of the 22 substrates tested, all but two (**29e** & **29f**) showed higher *Z* selectivity than expected from thermodynamic product ratios. 15 products showed greater than 1:1 *Z* selectivity. Aliphatic alkenes with 6- and 8-carbon chains have highest selectivity while the 10- and 12-carbon chains have the highest conversion. Coordination by heteroatoms or arenes may degrade selectivity and conversion, and understanding how these coordination modes change the mechanism will be critical to the expansion of *Z*-selective methods across multiple substrate classes.

Conclusion

We have studied the *Z*-selective isomerization of terminal alkenes with **3**. The available evidence suggests an allyl pathway through CO-assisted hydride migrations, where Z selectivity is the result of differences in steric pressure during rate determining pseudorotation. Migration could be a component of various catalytic transformations that require hydride rearrangement within a molecule, yet to be discovered. Our current efforts are focused on gaining experimental evidence for this unusual pathway and determining the prominence of similar mechanisms across other catalytic systems. We further seek an isomerization catalyst with a wider scope, with higher reactivity towards alkenes with Lewis basic functional groups, with an eye to efficient routes to highly functionalized building blocks in natural product synthesis, pharmaceuticals, and fragrances.

Experimental Section

Experimental Details. All manipulations were performed under N_2 atmosphere utilizing a Vacuum Atmospheres inert-atmosphere glovebox. NMR spectra were collected on Bruker Avance III 500 MHz and Avance IIIHD 500 MHz instruments. All ^{1}H and ^{13}C NMR chemical shifts (δ, ppm) were referenced to the residual protio-solvent peaks and deuterated solvent peaks, respectively. ^{31}P NMR spectra are referenced via external standard (H_3PO_4). Unless otherwise noted, commercial chemicals were used as received without further purification. Acetonitrile (CH_3CN), toluene (PhMe), dichloromethane (DCM), and pentane were purified using a commercial solvent purification system. Deuterated solvents were supplied by Cambridge Isotope Laboratories.

Computational Details. DFT calculations were performed in Gaussian 16, using M06-GD3/def2svp.[62–64] Vibrational frequencies were computed at the same level of theory to classify all stationary points as either saddle points (with a single imaginary frequency) or minima (with only real frequencies) and to obtain the thermochemical corrections at p=1 atm, T=298.15 K). The energies of the optimized geometries were then refined by single point calculations with a def2tzvp basis set.[64] The solvation effects of benzene were included in the energy refinements using the continuum SMD model (See SI for additional details).[65,66] The 1 M standard state energy correction[67–69] has been included in steps changing molecularity. The substrate used for the computation studies was 1-butene. Gibbs free energies are shown in kcal/mol. NBO analysis was performed using NBO 7.0.[70]

General Procedure for Catalytic Reactions. Unless otherwise noted, all reactions were run in triplicate and the reported conversion, yield, and selectivity represent an average of three trials. In a nitrogen atmosphere glovebox, an NMR tube was charged with 1.28 mmol of substrate. 400 µL of a stock solution containing 13.5 mM *cis*-$Mo(CO)_4(PCy_3)$(piperidine) (3.1 mg, 0.15 mol%) in C_6D_6 was added. 100 µL of a 60.0 mM stock solution of diphenyl phosphate (1.5 mg, 0.15 mol%) in C_6D_6 was added. The NMR tube was capped, removed from the glove box, and immersed in an 80 °C oil bath. NMR yield and selectivity were determined using ^{1}H NMR unless otherwise noted.

Procedure for Catalytic Reactions with (3) Formed In Situ. In a nitrogen atmosphere glovebox, a vial was charged with 7.68 mmol of substrate. *cis*-$Mo(CO)_4(piperidine)_2$ (2.9 mg, 0.1 mol%), tricyclohexylphosphine (2.1 mg, 1mol%), and diphenyl phosphate (2.0 mg, 0.1 mol%) was added. The solids were dissolved in 3 mL benzene (0.5 mL C_6D_6, 2.5 mL C_6H_6). The vial was capped, removed from the glove box, and immersed in an 80 °C oil bath. NMR yield and selectivity were determined using ^{1}H NMR.

Calculation of Conversion and Selectivity. Conversion was determined by comparing the ^{1}H NMR integrations of the alkenyl hydrogens in the starting material with those in the product. The selectivity is determined by comparing the ^{1}H NMR integrations of the terminal allylic hydrogens for the *Z*-2-alkene and *E*-2-alkene isomers. The conversion to 2-alkenes specifically was determined using the total integration of allylic hydrogens for *E*- and *Z*-2-alkenes, relative to one hydrogen, divided by the total integration of all alkenyl hydrogens present, relative to one hydrogen, per the equation

$$\frac{\frac{(E\text{-2 and } Z\text{-2 allyl hydrogens})}{3H}}{\frac{(\text{alkenyl hydrogens})}{2H}} = \text{2-alkenes}$$

The amount of other alkenes (e.g., 3-alkenes, 4-alkenes …) can be calculated as the difference between conversion and concentration of 2-alkene products. Note that in some cases, overlap of the *E*-2 and *Z*-2 peaks with another peak overlap requires the use of ^{13}C NMR to quantify *Z*:*E* and higher alkenes. An example of this calculation is provided in the Supporting Information.

Supporting Information

The authors have cited additional references within the Supporting Information.[71–74]

Acknowledgements

This work was supported by the National Science Foundation (CHE-1565721, CHE-2154438). Support for the NMR facility at Temple University by a CURE grant from the Pennsylvania

Department of Health is gratefully acknowledged. DFT studies were in part (A.N.) funded by the Research Council of Norway (project numbers 314321 and 262695). This research includes calculations carried out on HPC resources supported in part by the National Science Foundation through major research instrumentation grant number 1625061 and by the US Army Research Laboratory under contract number W911NF-16-2-0189.

Keywords: Isomerization • DFT • Molybdenum • Homogeneous Catalysis • Reaction Mechanisms

[1] A.-H. Obeid, J. Hannedouche, *Adv. Synth. Catal.* **2023**, *365*, 1100–1111.
[2] D. Kim, G. Pillon, D. J. Diprimio, P. L. Holland, *J. Am. Chem. Soc.* **2021**, *143*, 3070–3074.
[3] T. C. Cao, A. L. Cooksy, D. B. Grotjahn, *ACS Catal.* **2020**, *10*, 15250–15258.
[4] J. Becica, O. D. Glaze, D. I. Wozniak, G. E. Dobereiner, *Organometallics* **2018**, *37*, 482–490.
[5] S. W. M. Crossley, F. Barabe, R. A. Shenvi, *J. Am. Chem. Soc.* **2014**, *136*, 16788–16791.
[6] S. Zhang, D. Bedi, L. Cheng, D. K. Unruh, G. Li, M. Findlater, *J. Am. Chem. Soc.* **2020**, *142*, 8910–8917.
[7] D. Gauthier, A. T. Lindhardt, E. P. K. Olsen, J. Overgaard, T. Skrydstrup, *J. Am. Chem. Soc.* **2010**, *132*, 7998–8009.
[8] A. M. Camp, M. R. Kita, P. T. Blackburn, H. M. Dodge, C. H. Chen, A. J. M. Miller, *J. Am. Chem. Soc.* **2021**, *143*, 2792–2800.
[9] J. J. Molloy, T. Morack, R. Gilmour, *Angew. Chem. - Int. Ed.* **2019**, *58*, 13654–13664.
[10] E. Kudo, K. Sasaki, S. Kawamata, K. Yamamoto, T. Murahashi, *Nat. Commun.* **2021**, *12*, 1–8.
[11] M. C. Aguilera, M. L. Neidig, *Chem Catal.* **2021**, *1*, 488–489.
[12] X. Yu, H. Zhao, P. Li, M. J. Koh, *J. Am. Chem. Soc.* **2020**, *142*, 18223–18230.
[13] S. Garhwal, A. Kaushansky, N. Fridman, G. Ruiter, *Chem Catal.* **2021**, *1*, 631–647.
[14] H. Iwamoto, T. Tsuruta, S. Ogoshi, *ACS Catal.* **2021**, *11*, 6741–6749.
[15] S. Gao, J. Chen, M. Chen, *Chem. Sci.* **2019**, *10*, 3637–3642.
[16] B. A. Kustiana, S. A. Elsherbeni, T. G. Linford-Wood, R. L. Melen, M. N. Grayson, L. C. Morrill, *Chem. – Eur. J.* **2022**, *28*, e202202454.
[17] R. S. Phatake, T. Müller, A. Averdunk, U. Gellrich, *Org Chem Front* **2023**, *10*, 1128–1133.
[18] S. De-Botton, D. Sc. O. A. Filippov, E. S. Shubina, N. V. Belkova, D. Gelman, *ChemCatChem* **2020**, *12*, 5959–5965.
[19] A. Vasseur, J. Bruffaerts, I. Marek, *Nat. Chem.* **2016**, *8*, 209–219.
[20] T. C. Jankins, R. Martin-Montero, P. Cooper, R. Martin, K. M. Engle, *J. Am. Chem. Soc.* **2021**, *143*, 14981–14986.
[21] I. Massad, I. Marek, *ACS Catal.* **2020**, *10*, 5793–5804.
[22] Y. Siau, W.-Y.; Zhang, Y.; Zhao, *Stereoselective Synthesis of Z- Alkenes. In Stereoselective Alkene Synthesis*, Springer, Berlin, **2012**.
[23] J. Pollini, W. M. Pankau, L. J. Gooßen, *Chem. - Eur. J.* **2019**, *25*, 7416–7425.
[24] T. L. Lohr, T. J. Marks, *Nat. Chem.* **2015**, *7*, 477–482.
[25] C. R. Larsen, D. B. Grotjahn, in *Appl. Homog. Catal. Organomet. Compd.*, **2017**, pp. 1365–1378.
[26] K. Mackenzie, in *Chem. Alkenes*, **1964**, pp. 387–467.
[27] R. C. Larock, Ed. , *Comprehensive Organic Transformations: A Guide to Functional Group Preparations*, John Wiley & Sons, New York, **2018**.
[28] M. Beller, J. Seayad, A. Tillack, H. Jiao, *Angew. Chem. Int. Ed.* **2004**, *43*, 3368–3398.
[29] K. Singh, S. J. Staig, J. D. Weaver, *J. Am. Chem. Soc.* **2014**, *136*, 5275–5278.
[30] C. Cruch, W. Neiderer, S. K. Collins, *ACS Catal.* **2021**, *11*, 8829–8836.
[31] J. B. Metternich, R. Gilmour, *J. Am. Chem. Soc.* **2015**, *137*, 11254–11257.
[32] C. Rubel, A. Ravn, S. Yang, Z.-Q. Li, K. M. Engle, J. Vantourout, *ChemRxiv Prepr.* **2022**, 10.26434/chemrxiv-2022-x8ssk.
[33] C. Chen, T. R. Dugan, W. W. Brennessel, D. J. Weix, P. L. Holland, *J. Am. Chem. Soc.* **2014**, *136*, 945–955.
[34] A. Schmidt, A. R. Nödling, G. Hilt, *Angew. Chem. Int. Ed.* **2015**, *54*, 801–804.
[35] F. Weber, A. Schmidt, P. Röse, M. Fischer, O. Burghaus, G. Hilt, *Org. Lett.* **2015**, *17*, 2952–2955.
[36] F. Pünner, A. Schmidt, G. Hilt, *Angew. Chem. Int. Ed.* **2012**, *51*, 1270–1273.
[37] S. Xu, P. Geng, Y. Li, G. Liu, L. Zhang, Y. Guo, Z. Huang, *ACS Catal.* **2021**, *11*, 10138–10147.
[38] A. Scarso, M. Colladon, P. Sgarbossa, C. Santo, R. A. Michelin, G. Strukul, D. Chimica, V. Marzolo, P. Chimici, *Organometallics* **2010**, 1487–1497.
[39] T. C. Morrill, C. A. D'Souza, *Organometallics* **2003**, *22*, 1626–1629.
[40] P. W. N. M. van Leeuwen, *Homogeneous Catalysis: Understanding the Art*, Kluwer Academic Publishers, Boston, **2004**.
[41] S. Biswas, *Comments Inorg. Chem.* **2015**, *35*, 300–330.
[42] R. H. Crabtree, *The Organometallic Chemistry of the Transition Metals*, Wiley, Hoboken, **2014**.
[43] S. M. Casey, C.P.; Neumann, *J. Am. Chem. Soc.* **1976**, *98*, 5395–5396.
[44] P. C. Pearson, R.G.; Walker, H.W.; Mauermann, H.; Ford, *Inorg. Chem.* **1981**, *20*, 2741–2743.
[45] Ö. Öztopcu, C. Holzhacker, M. Puchberger, M. Weil, K. Mereiter, L. F. Veiros, K. Kirchner, *Organometallics* **2013**, *32*, 3042–3052.
[46] D. J. Darensbourg, R. L. Kump, *Inorg. Chem.* **1978**, *17*, 2680–2682.
[47] J. E. Cortés-Figueroa, L. Santiago, M. S. León, M. P. De Jesús, *J. Coord. Chem.* **1997**, *41*, 249–259.
[48] J. N. Harvey, F. Himo, F. Maseras, L. Perrin, *ACS Catal.* **2019**, *9*, 6803–6813.
[49] A. Kapat, T. Sperger, S. Guven, F. Schoenebeck, *Science* **2019**, *363*, 391–396.
[50] M. Baya, P. A. Dub, J. Houghton, J.-C. Daran, N. V. Belkova, E. S. Shubina, L. M. Epstein, A. Lledós, R. Poli, *Inorg. Chem.* **2009**, *48*, 209–220.
[51] J. A. R. Luft, Z. X. Yu, D. L. Hughes, G. C. Lloyd-Jones, S. W. Krska, K. N. Houk, *Tetrahedron Asymmetry* **2006**, *17*, 716–724.
[52] S. Asako, S. Ishikawa, K. Takai, *ACS Catal.* **2016**, *6*, 3387–3395.
[53] Y. D. Ward, L. A. Villanueva, G. D. Allred, S. C. Payne, M. A. Semones, L. S. Liebeskind, *Organometallics* **1995**, *14*, 4132–4156.
[54] A. Nova, G. Ujaque, A. C. Albéniz, P. Espinet, *Chem. - Eur. J.* **2008**, *14*, 3323–3329.
[55] C. C. Yang, W. Y. Yeh, G. H. Lee, S. M. Peng, *J. Organomet. Chem.* **2000**, *598*, 353–358.
[56] F. Basolo, *Polyhedron* **1990**, *9*, 1503–1535.
[57] D. M. P. Mingos, *J. Organomet. Chem.* **1979**, *179*, 29–33.
[58] D. Balcells, F. Maseras, *New J. Chem.* **2007**, *31*, 333–343.
[59] S. M. M. Knapp, S. E. Shaner, D. Kim, D. Y. Shopov, J. A. Tendler, D. M. Pudalov, A. R. Chianese, *Organometallics* **2014**, *33*, 473–484.
[60] E. Taskinen, N. Lindholm, *J. Phys. Org. Chem.* **1994**, *7*, 256–258.
[61] W. G. Young, J. S. Franklin, *J. Am. Chem. Soc.* **1966**, *88*, 785–790.
[62] M. J. Frisch, G. W. Trucks, H. B. Schlegel, G. E. Scuseria, M. A. Robb, J. R. Cheeseman, G. Scalmani, V. Barone, G. A. Petersson, H. Nakatsuji, X. Li, M. Caricato, A. V. Marenich, J. Bloino, B. G. Janesko, R. Gomperts, B. Mennucci, H. P. Hratchian, J. V. Ortiz, A. F. Izmaylov, J. L. Sonnenberg, D. Williams-Young, F. Ding, F. Lipparini, F. Egidi, J. Goings, B. Peng, A. Petrone, T. Henderson, D. Ranasinghe, V. G. Zakrzewski, J. Gao, N. Rega, G. Zheng, W. Liang, M. Hada, M. Ehara, K. Toyota, R. Fukuda, J. Hasegawa, M. Ishida, T. Nakajima, Y. Honda, O. Kitao, H. Nakai, T. Vreven, K. Throssell, J. A. Montgomery Jr., J. E. Peralta, F. Ogliaro, M. J. Bearpark, J. J. Heyd, E. N. Brothers, K. N. Kudin, V. N. Staroverov, T. A. Keith, R. Kobayashi, J. Normand, K. Raghavachari, A. P. Rendell, J. C. Burant, S. S. Iyengar, J. Tomasi, M. Cossi, J. M. Millam, M. Klene, C. Adamo, R. Cammi, J. W. Ochterski, R. L. Martin, K. Morokuma, O. Farkas, J. B. Foresman, D. J. Fox, *Gaussian-16*, Gaussian, Inc., Wallingford, CT, **2016**.
[63] Y. Zhao, D. G. Truhlar, *Theor. Chem. Acc.* **2008**, *120*, 215–241.
[64] F. Weigend, R. Ahlrichs, *Phys. Chem. Chem. Phys.* **2005**, *7*, 3297–3305.
[65] W. Kohn, A. D. Becke, R. G. Parr, *J. Phys. Chem.* **1996**, *100*, 12974–12980.
[66] A. Marenich, C. J. Cramer, D. G. Truhlar, *J. Phys. Chem. B* **2009**, *113*, 6378–6396.

[67] G. Norjmaa, A. Solé-Daura, M. Besora, J. M. Ricart, J. J. Carbó, *Inorg. Chem.* **2021**, *60*, 807–815.
[68] M. Mammen, E. I. Shakhnovich, J. M. Deutch, G. M. Whitesides, *J. Org. Chem.* **1998**, *63*, 3821–3830.
[69] A. Ishikawa, Y. Nakao, H. Sato, S. Sakaki, *Inorg. Chem.* **2009**, *48*, 8154–8163.
[70] E. D. Glendening, J. K. Badenhoop, A. E. Reed, J. E. Carpenter, J. A. Bohmann, C. M. Morales, P. Karafiloglou, C. R. Landis, F. Weinhold, *NBO 7.0*, Theoretical Chemistry Institute, University of Wisconsin, Madison, **2018**.
[71] G. J. Kubas, *J. Chem. Soc. Chem. Commun.* **1980**, 61–62.
[72] J. E. Cortes-Figueroa, M. S. Leon-Velazquez, J. Ramos, J. P. Jasinski, D. A. Keene, J. D. Zubkowski, E. J. Valente, *Acta Crystallogr. Sect. C* **2000**, *56*, 1435–1437.
[73] G. A. Molander, D. L. Sandrock, *J. Am. Chem. Soc.* **2008**, *130*, 15792–15793.
[74] D. A. L. Otte, D. E. Borchmann, C. Lin, M. Weck, K. A. Woerpel, *Org. Lett.* **2014**, *16*, 1566–1569.

Entry for the Table of Contents

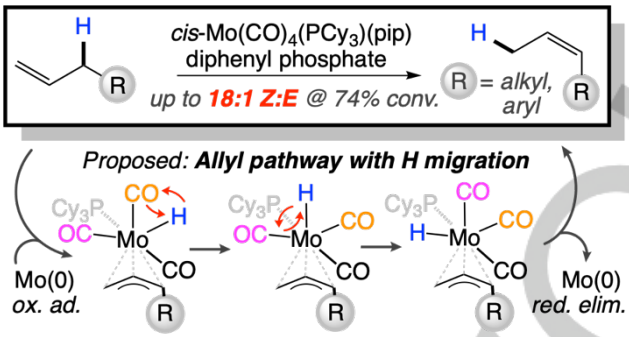

Selective isomerization of terminal alkenes to *Z*-2-alkenes is challenging because of the thermodynamic preference for *E* alkenes. This work investigates the mechanism of a Mo catalyst that achieves high *Z* selectivity for a range of aliphatic alkenes. DFT analysis points to a hydride migration as key to the isomerization process.

Institute and/or researcher Twitter usernames: @TUChemBot